IOPscience iopscience.iop.org

Home Search Collections Journals About Contact us My IOPscience

Defect mediated photocatalytic decomposition of 4-chlorophenol on epitaxial rutile thin films under visible and UV illumination

This article has been downloaded from IOPscience. Please scroll down to see the full text article.

2012 J. Phys.: Condens. Matter 24 395005

(http://iopscience.iop.org/0953-8984/24/39/395005)

View the table of contents for this issue, or go to the journal homepage for more

Download details:
IP Address: 128.219.49.13
The article was downloaded on 30/10/2012 at 19:11

Please note that terms and conditions apply.

IOP PUBLISHING JOURNAL OF PHYSICS: CONDENSED MATTER

J. Phys.: Condens. Matter **24** (2012) 395005 (9pp) doi:10.1088/0953-8984/24/39/395005

Defect mediated photocatalytic decomposition of 4-chlorophenol on epitaxial rutile thin films under visible and UV illumination

M R Bayati[1], J Ding[2], Y F Lee[1], R J Narayan[1,3], J Narayan[1], H Zhou[4] and S J Pennycook[4]

[1] Department of Materials Science and Engineering, North Carolina State University, EB-1, Raleigh 27695-7906, NC, USA
[2] Department of Materials Science and Engineering, Zhejiang University, Hangzhou 310027, People's Republic of China
[3] Joint Department of Biomedical Engineering, UNC Chapel Hill and North Carolina State University, EB-3, Raleigh 27695-7115, NC, USA
[4] Materials Science and Technology Division, Oak Ridge National Laboratory, Oak Ridge, TN 37831, USA

E-mail: mbayati@ncsu.edu

Received 9 June 2012, in final form 1 August 2012
Published 3 September 2012
Online at stacks.iop.org/JPhysCM/24/395005

Abstract
We show that pure rutile TiO_2 can be photo-responsive even under low energy visible light after annealing in vacuum where we envisage that the point defects, i.e. oxygen vacancies and titanium interstitials, serve an important role. In this study, single crystal rutile films were grown by the pulsed laser deposition technique and then vacuum annealed under different oxygen pressures to introduce defects into their lattices. 4-chlorophenol was selected as a model material and decomposed by the annealed TiO_2 films where the maximum photocatalytic reaction rate constants were determined as 0.0107 and 0.0072 min^{-1} under UV and visible illumination. Epitaxial growth along the [200] direction was confirmed by φ-scan and 2θ-scan XRD and the epitaxial relationship between the rutile film and the c-sapphire substrate was explained as $(100)[010]_R \parallel (0001)[1\bar{2}10]_S$. The formation of atomically sharp interfaces and the epitaxial growth were ascertained by annular dark-field STEM imaging. Based on the XPS, UV–vis and PL spectroscopy results, it was found that the defect concentration increased after annealing under lower pressures, e.g. 5×10^{-6} Torr. In contrast, more perfect crystals were obtained when the films were annealed under high oxygen pressures, namely 5×10^{1} Torr. The morphology of the films was also investigated by employing an AFM technique. It was observed that increase of the annealing pressure results in the formation of larger grains. It was also found that the electrical resistivity of the rutile films strongly increased by about three orders of magnitude when the annealing pressure increased from 5×10^{-4} to 5×10^{1} Torr.

(Some figures may appear in colour only in the online journal)

1. Introduction

Chlorinated phenolic compounds are characterized by high toxicity even at relatively low concentration and persistency in both water and soils. They are usually released to the environment by pulp and paper manufacturers, oil refining activities and textile industries. In particular, 4-chlorophenol (4CP) can originate from the chlorination processes of

 © 2012 IOP Publishing Ltd Printed in the UK & the USA

phenol containing wastewater or from the breakdown of pesticides and chlorinated aromatic compounds. Moreover, it is an intermediate by-product in the production of 2, 4-dichlorophenol and 4-chlorophenol-o-cresol. The latter can be oxidized by chemical, photochemical and microbiological processes. Photocatalytic decomposition of 4CP has been considered as a promising technique where the toxic material is mineralized to harmless products of CO_2 and H_2O. During this process, the 4CP molecules are degraded mainly by the attack of the • OH radical [1–3].

Among many kinds of photocatalyst material, titanium dioxide (TiO_2) has been widely studied and attracted considerable attention during the last decade, since it has superior physical and chemical properties. To enhance the photocatalytic efficiency, it is necessary to understand the principles of the photocatalytic reactions. In such reactions, first, the semiconductor is illuminated by light whose energy should be larger than the band gap energy of the semiconductor ($h\nu \geq E_g$). Then, electrons are excited from the valence band to the conduction band and, hence, holes are generated in the valence band. This process makes electron–hole pairs which are a prerequisite for photocatalytic applications [4, 5],

$$\mathrm{SP} + h\nu \longrightarrow \mathrm{SP}(\mathrm{h}^+ + \mathrm{e}^-). \tag{1}$$

Afterward, the photogenerated electron–hole pairs chemically react with the adsorbed water and oxygen molecules to create high energy $OH^\bullet$ and $O_2^{\bullet-}$ radicals,

$$\mathrm{O}_{2(\mathrm{ads})} + \mathrm{e}^- \longrightarrow \mathrm{O}_2^{\bullet-} \tag{2}$$

$$\mathrm{H}_2\mathrm{O} + \mathrm{h}^+ \longrightarrow \mathrm{H}^+ + \mathrm{OH}^\bullet \tag{3}$$

$$\mathrm{O}_2^{\bullet-} + \mathrm{H}^+ \longrightarrow \mathrm{HO}_2^{\bullet-} \tag{4}$$

$$2\mathrm{HO}_2^{\bullet-} \longrightarrow \mathrm{H}_2\mathrm{O}_2 + \mathrm{O}_2 \tag{5}$$

$$\mathrm{H}_2\mathrm{O}_2 + h\nu \longrightarrow 2\mathrm{OH}^\bullet. \tag{6}$$

The $OH^\bullet$ and $O_2^{\bullet-}$ radicals, generated through the above reactions, are very energetic and active. As strong oxidizing and reducing agents, they have impressive chemical activities which can decompose both organic and inorganic molecules efficiently. Regarding the aforementioned mechanism, the generation and separation of e^-–h^+ pairs are the critical steps of any photocatalytic reaction. Since the band gap energy of TiO_2 is 3.0–3.2 eV, only the ultraviolet part of the solar radiation (about 4% of the total solar energy reaching the Earth's surface) can excite TiO_2 to generate e^-–h^+ pairs. This, to some extent, limits practical applications of TiO_2. To date, several studies have been carried out to enhance the catalytic efficiency under visible light and different solutions have been proposed such as doping and combining titania with metallic elements, non-metallic elements and other semiconductors [6–11]. Another way, which has not been investigated thoroughly, is based on introduction of point defects to the crystalline lattice of TiO_2. Such defects might alter the energy bands of the semiconductor by introducing defect energy levels within the band gap resulting in band gap narrowing. There are six different kinds of point defect in the TiO_2 structure, namely titanium interstitial (Ti_i), titanium vacancy (V_{Ti}), oxygen interstitial (O_i), oxygen vacancy (V_O) and two anti-site defects, Ti_O and O_{Ti}. Each of these defects has a specific formation energy (ΔH) under titanium and oxygen rich growth conditions. The theoretical estimations of formation energies of anti-site and titanium vacancy defects are too high. They form merely under extreme conditions due to the large cation–anion size mismatch and strong iconicity of the material. However, the formation energies of Ti_i and V_O defects are about 2–3 eV under Ti-rich (low oxygen partial pressure) growth conditions, respectively. As a result, V_O and Ti_i defects are the most probable structural defects of TiO_2 [12]. From the kinetics viewpoint, the formation of V_O is more favored than Ti_i. Both V_O and Ti_i defects introduce energy levels inside the band gap of titania and play a significant role in increasing the absorbance in the visible region. It is worth mentioning that the Ti_i defect has two different types, Ti_i^{4+} and Ti_i^{3+}. The fingerprint of the formation of Ti^{3+} ions is an energy band edge at about 2 eV above the valence band maximum and about 1 eV below the conduction band minimum [13]. The defects, no matter whether they are located at the surface or at the interface, are considered to act as functional electron traps to reduce the recombination of electrons and holes, resulting in a promoted photoactivity of TiO_2 films [14]. Oxygen vacancies can form defect centers serving as electron traps and, thus, promote charge transfer [15]. As a consequence, defects can decrease the recombination rate of e^-–h^+ pairs resulting in an improvement in photocatalytic activity.

It is well known that the competition among the recombination, trapping and transfer of photogenerated electron–hole pairs determines the overall photocatalytic efficiency. To achieve a high photocatalytic efficiency in TiO_2 films, the e^-–h^+ pairs should be effectively extracted to the surface without recombination. Inasmuch as grain boundaries can scatter or trap the photogenerated electrons and holes and act as charge recombination centers, reduction of grain boundaries and growth of single crystal films lead to the formation of highly photoactive TiO_2 films.

In this paper, we report the growth and characterization of single crystal rutile TiO_2 films on *c*-cut sapphire where our emphasis is placed on introducing structural point defects to the crystalline lattices of the films through annealing them under vacuum. We will show that the defect content as well as the photocatalytic performance of the films can be appropriately tuned by changing the annealing pressure. It will be also shown that the pure rutile films, annealed under low pressures, are responsive under visible light where we envisage that point defects play a major role.

2. Experimental procedure

Epitaxial rutile TiO_2 films were deposited on single crystal *c*-cut sapphire ($A1_2O_3$) substrates by a PLD technique. Prior to deposition, the substrates were cleaned through a multi-step procedure including boiling in acetone at 150 °C for 15 min and ultrasonic cleaning in acetone for 5 min followed by ultrasonic cleaning in methanol for 5 min. Finally, the cleaned

substrates were fully dried by nitrogen gun and loaded into the PLD chamber. A Lambda Physik (LPX200) KrF excimer laser ($\lambda = 248$ nm, $\tau = 25$ ns) was employed to ablate the TiO_2 target. The target was rotated during the deposition to provide a uniform ablation and avoid any pitting on its surface. Before injecting oxygen into the chamber, the chamber was evacuated to a background pressure of $\sim 1 \times 10^{-6}$ Torr. The laser energy, shot frequency, oxygen pressure, growth time and substrate temperature were the same for all samples and were considered to be $\sim$3.5 J cm^{-2}, 10 Hz, 5×10^{-4} Torr , 20 min and 450 °C, respectively. Immediately after deposition, the layers were subjected to vacuum annealing inside the PLD chamber for 1 h at 450 °C under different pressures of 5×10^{-6} to 5×10^{1} Torr with 10^{1} intervals.

The crystalline structure of theTiO_2 films was investigated by 2θ XRD scanning using a Rigaku x-ray diffractometer with Cu Kα radiation ($\lambda = 0.154$ nm). A Philips X'Pert Pro x-ray diffractometer was also employed for φ-scanning to determine the in-plane and out-of-plane orientations of the TiO_2 films. The morphology of the layers was studied by a Veeco AFM as well and the results were interpreted by nanoscope ver. 5.12r3 software. The optical properties of the films were studied by a U-3010 Hitachi UV–vis spectrophotometer. The room temperature photoluminescence (PL) spectra of the samples were recorded with a fluorescence spectrophotometer (Hitachi, F-2500) using an excitation wavelength of 300 nm. Annular dark-field scanning transmission electron microscopy (ADF-STEM) imaging with a Nion UltraSTEM 200 operated at 200 keV was used to confirm the epitaxial growth of the layers. To determine the surface chemical composition and stoichiometry of the layers, x-ray photoelectron spectroscopy (XPS) was performed employing a Riber instrument with a Mg Kα x-ray source. The samples were sputtered by Ar^+ bombardment for 5 min prior to acquiring data to remove any probable surface contamination. Interpretation of the XPS results was performed using the SDP ver. 4.1 software. The electrical properties of the films were studied using a self-made labview program employing a Keithley 2400 sourcemeter. The measurements were made in a temperature range of 242–342 K. The samples were cooled using a closed cycle helium cryostat. Using a Tencor Alpha Step stylus profilometer, the thickness of the films was determined to be about 300 nm.

The photocatalytic activity of the layers was evaluated by measuring the degradation rate of aqueous 4-chlorophenol (4CP) solution at room temperature. 50 ml of the 4CP solution (2×10^{-4} M) and a 1 cm × 1 cm sample, as a photocatalyst, were placed in a beaker. A medium pressure mercury lamp ($\lambda = 200$–300 nm) was used as the ultraviolet source during the photocatalytic experiments. Prior to UV irradiation, in each experiment, the solution and the catalyst were left in the dark for 30 min (considered as a reference point) until adsorption/desorption equilibrium was reached. The solution was then irradiated by UV light. A UV–vis spectrophotometer (Hitachi, U-3010) was used to measure the change in concentration, based on the Beer–Lambert equation which states $A = \varepsilon \times b \times C$ where A, ε, b and C are the absorptance of the solution, molar absorptivity, path length and solution concentration, respectively. Using a quartz cell, a fixed quantity of the solution was removed every 20 min to measure the absorption and then the concentration at a fixed wavelength of 230 nm. To evaluate the visible photocatalytic efficiency of the TiO_2 films, a similar set of experiments was conducted under visible light using a halogen lamp where the shorter wavelengths ($\lambda < 420$ nm) were cut off by a UV filter.

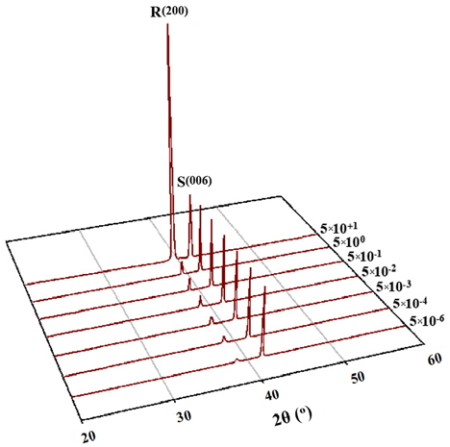

Figure 1. XRD patterns of the rutile films annealed under various pressures.

3. Results and discussion

Figure 1 shows XRD patterns of the rutile TiO_2 films annealed under different pressures where the formation of epitaxial or highly textured films is evident. The as-deposited samples had a rutile structure as well (data not shown here). It was found that the rutile (200) characteristic peak gets more intense at higher annealing pressures. Simultaneously, the full width at half maximum (FWMH) decreases when the grown films are annealed under higher pressures. In other words, layers with more favorable crystallinity and better quality were obtained after annealing under higher pressures. As was discussed earlier, oxygen vacancies (V_O) and titanium interstitials (Ti_i) are two most important intrinsic defects in TiO_2. The formation of these point defects in TiO_2 may be described by the following reactions [16–18]:

$$O_O \rightleftharpoons V_O + 2e^- + 1/2O_2 \quad (7)$$

$$2O_O + Ti_{Ti} \rightleftharpoons Ti_i^{3+} + 3e^- + O_2 \quad (8)$$

$$2O_O + Ti_{Ti} \rightleftharpoons Ti_i^{4+} + 4e^- + O_2. \quad (9)$$

Regarding reactions (7)–(9), the concentration of the lattice defects may be expressed as a function of $p(O_2)$ as follows [19]:

$$[V_O] \propto p(O_2)^{-1/2} \quad (10)$$

$$[Ti_i^{3+}] \propto p(O_2)^{-1} \quad (11)$$

$$[Ti_i^{4+}] \propto p(O_2)^{-1}. \quad (12)$$

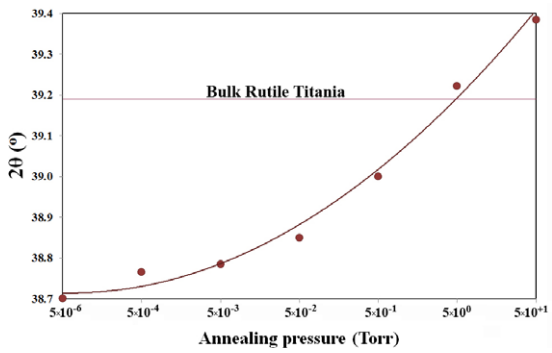

Figure 2. The diffraction angle (2θ) of the rutile (200) peak as a function of the annealing pressure.

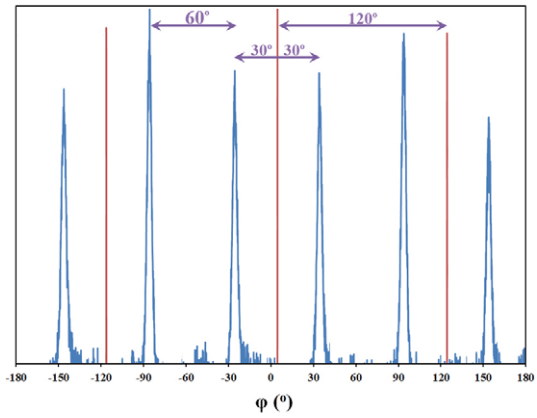

Figure 3. The φ-scan XRD pattern of the rutile TiO_2 sample on *c*-cut sapphire (red: sapphire $(01\bar{1}2)$ and blue: rutile (110) reflections).

Considering these equations, it can be concluded that the oxygen pressure plays an important role in the formation or removal of these point defects in the TiO_2 crystalline structure. It can be also suggested that annealing of the films under higher oxygen partial pressures results in a decreasing concentration of point defects in the grown samples. As a consequence, rutile films with better quality were obtained at higher annealing pressures, i.e. 5×10^1 Torr. The structural factor increases when point defects are removed leading to the appearance of more intense and sharper XRD peaks. High resolution XRD was also carried out to determine the exact 2θ values of the rutile (200) peak, the results of which are presented in figure 2. As is seen, the rutile (200) peak shifts toward smaller 2θ values when the layers are annealed under lower pressures. This peak shift can be assigned to the formation of more defects which results in change of the *d*-spacing between the planes.

To confirm the growth of single crystal rutile films, XRD φ-scanning was carried out on the $(01\bar{1}2)$ reflection plane ($2\theta = 25.58°$, $\psi = 57.70°$) of the sapphire substrate and the (110) reflection plane ($2\theta = 27.44°$, $\psi = 45.00°$) of the rutile film (figure 3). Due to the threefold symmetry of the sapphire (0001) substrate with a hexagonal lattice, three $(01\bar{1}2)$ reflection peaks with 120° intervals were observed. In addition, six strong symmetrical peaks appeared with angular intervals of 60° for the (110) family of planes of the film. This indicates that three different grain orientations are present in the rutile film which is due to the threefold symmetry in the pseudo-hexagonal structure of the (0001) sapphire substrate. Thus, the formation of the threefold mosaic structure in the epitaxial (200) TiO_2 rutile film was due to the nucleation and growth of the three variants on the sapphire (0001) substrate [20]. As was already shown in our previous works [21, 22], the epitaxial relationship was established as rutile (100) ∥ sapphire(0001), rutile [001] ∥ sapphire $[10\bar{1}0]$ and rutile [010] ∥ sapphire $[1\bar{2}10]$. Since the films were grown epitaxially, the grain boundaries present in the films have low angles which show lower scattering effects against electron–hole pairs [23]. The proposed epitaxial relationship, columnar growth and in-plane 60° rotation are further confirmed by high resolution ADF-STEM imaging as shown in figures 4(a) and (b) where the formation of an atomically sharp interface between the film and the substrate is also observed. In-plane rotation of the rutile grains is also evident. Epitaxial films are expected to exhibit significantly higher photocatalytic efficiencies, because their charge carriers have higher mobility and can diffuse to the surface of the catalyst without scattering to participate in the catalytic reactions (equations (1)–(6)), as discussed earlier.

The surface morphology of the rutile films, determined by AFM, is depicted in figure 5. It is seen that the surface roughness increases when the oxygen pressure of the annealing process increases from 5×10^{-6} to 5×10^1 Torr. The surface roughness was determined to be 4.26, 5.31, 6.01, 9.13, 18.86 and 23.32 nm for annealing pressures of $5 \times 10^{-6}, 5 \times 10^{-4}, 5 \times 10^{-3}, 5 \times 10^{-2}, 5 \times 10^0$ and 5×10^1 Torr, respectively. We already saw that most of the structural defects were removed after annealing under high oxygen pressures, namely 5×10^1 Torr. Since the defects tend to accumulate around grain boundaries, the grain boundaries are to some extent confined by them and cannot migrate freely. That is, their migration needs a higher energy. However, after annealing under higher pressures and, hence, reducing the defect content, the grain boundaries can migrate more easily, so larger grains form. We showed that the grown films are single crystal and the grain boundaries are small angle boundaries. That is, the adjacent grains are crystallographically continuous.

Room temperature PL spectra of the rutile films are displayed in figure 6. All emissions having wavelengths shorter than 420 nm were eliminated by a filter to highlight the peaks from the energy levels of defects. The wide emission peak at a wavelength of ∼450 nm is attributed to the oxygen vacancy energy levels. The PL intensities can be related to the recombination rate between the photogenerated electrons and holes. Since the charge carriers are trapped by defects, low PL intensity reveals a lower recombination rate and, thus, a higher defect concentration. Taking the PL results into closer consideration, it is suggested that annealing the rutile films under higher oxygen pressures leads to removal of the point defects or decrease of their concentration. UV–vis spectroscopy was employed to study the influence of vacuum

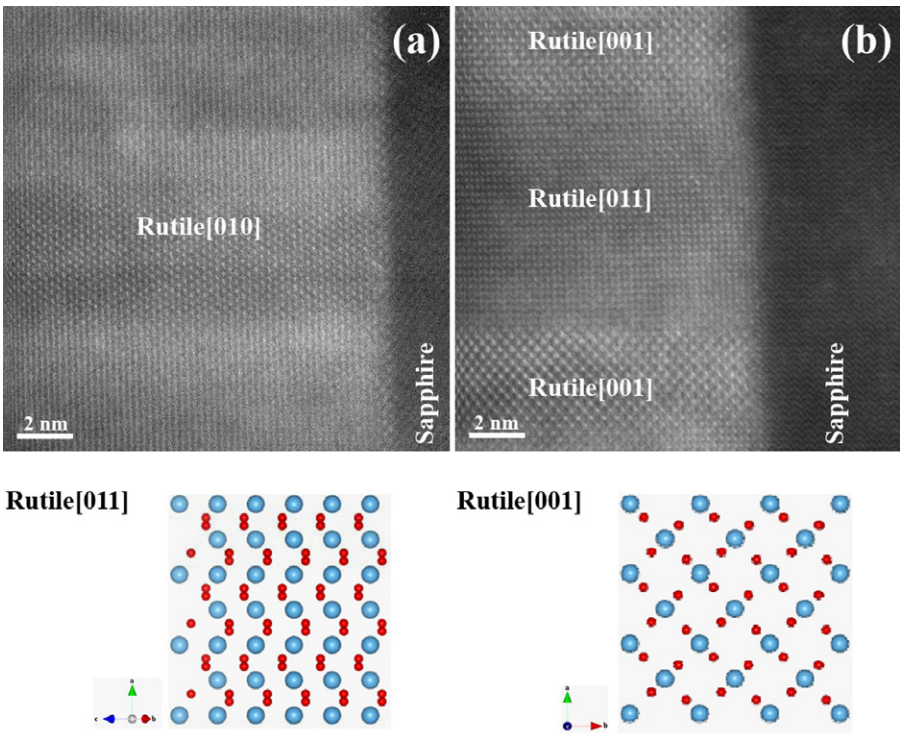

Figure 4. A high resolution ADF-STEM image showing (a) the $[1\bar{2}10]$ and (b) the $[10\bar{1}0]$ zone of *c*-sapphire.

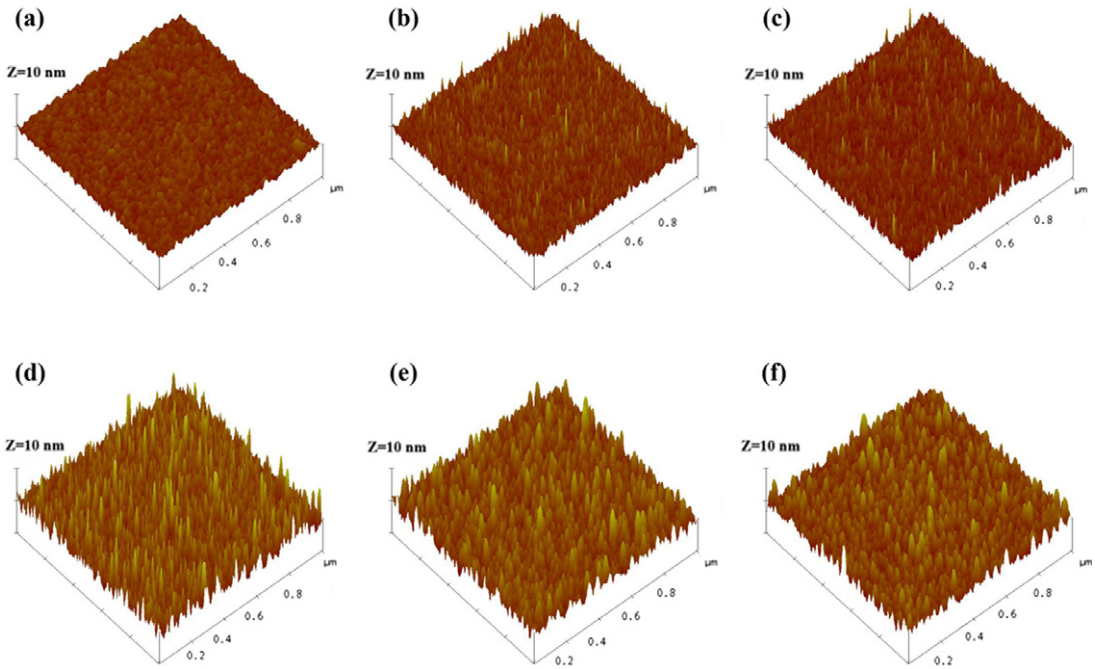

Figure 5. The effect of annealing pressure on the AFM surface morphology of the TiO_2 films: (a) 5×10^{-6}, (b) 5×10^{-4}, (c) 5×10^{-3}, (d) 5×10^{-2}, (e) 5×10^{0} and (f) 5×10^{1} Torr.

annealing on the optical properties of the films and the results are shown in figure 7. The films annealed under higher pressures are more transparent and their transmittance is about 85% which further confirms the formation of higher quality films after high oxygen pressure annealing. However, according to equations (10)–(12), the concentration of point defects increases at lower pressures. This phenomenon results in decrease of the transmittance, since these defects act as scattering centers for the incoming photons. Moreover, the films annealed under higher pressures exhibit a sharper absorbance edge which confirms lower defect content in these layers. It is also important to note that the transmittance

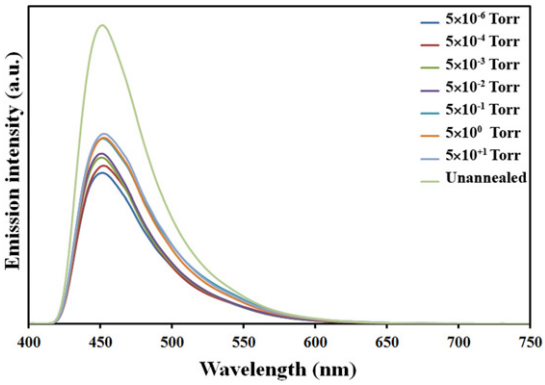

Figure 6. The influence of the annealing pressure on the room temperature PL spectra of the rutile films.

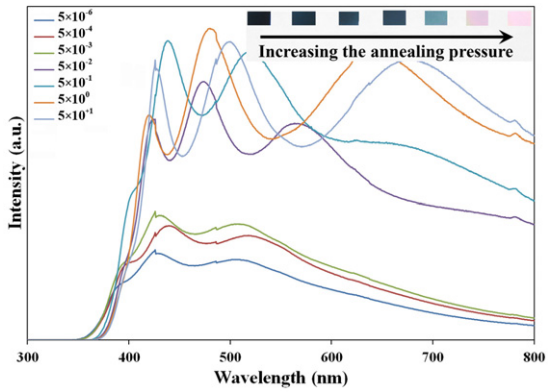

Figure 7. The transmittance spectra of the layers annealed under various oxygen pressures.

spectra of the rutile films annealed at lower pressures have an absorbance edge at ∼425 nm. That is, these films have a narrower band gap. We attribute this band gap narrowing to the introduction of Ti_i defects. The formation of Ti^{3+} cations gives rise to formation of a band edge in between the conduction and valence bands of titania. This energy level is located about 2 eV above the valence band maximum and about 1 eV below the bottom of the conduction band. As is shown in the inset of figure 7, the samples annealed at low pressures assume a bluish color whose intensity is a measure of the level of reduction and is assigned to d–d transitions [13, 18, 24].

The above studies on defect characteristics in the layers were completed by the XPS technique. Figures 8(a)–(c) show the O(1s) core level binding energy for the rutile films annealed under various pressures. Meanwhile, the O(1s) core level of the un-annealed layer is depicted in figure 8(d), as a reference. As is seen, the XPS peaks have been deconvoluted into distinct peaks using a Gaussian function. Peak A with a binding energy of ∼531.8 eV corresponds to the O^{2-} ions in oxygen deficient regions and its fraction scales with the concentration of oxygen vacancies (V_O). When an oxygen vacancy forms, the nearby Ti atoms relax outward, so the neighboring Ti–O bonds are shortened resulting in an increase of the bonding energy. As a consequence of the formation of the (V_O) defect, two Ti^{4+} ions have to get converted to Ti^{3+} ions to preserve the charge neutrality. In other words, Ti^{4+} ions trap two electrons that are generated when a V_O defect forms (equation (7)). Indeed, peak A is assigned to the oxygen deficient regions and can be attributed to the V_O defects. Peak B, located at a binding energy of 530.2 eV, is assigned to the oxygen ions in the crystalline lattice of perfect TiO_2. Peaks C and D, which have binding energies of about 528.0 and 526.9 eV respectively, may represent oxygen atoms in contact with Ti_i^{3+} and Ti_i^{4+} defects. When a titanium interstitial resides in the rutile lattice, it attracts the electron cloud between neighboring Ti and O atoms, leading to a decrease in energy of neighboring Ti–O bonds. A small peak shift is also observed for all these peaks due to variation of defect concentrations. Taking the peak portions into consideration (table 1), it can be suggested that the amount of lattice disorder, which is represented by peaks A, C and D, increases when the films are annealed under lower oxygen pressures. It is worth pointing out that peaks C and D are merged together in figures 8(c) and (d), since the concentrations of Ti_i^{3+} and Ti_i^{4+} defects in the un-annealed sample as well as the sample annealed under a pressure of 5×10^1 Torr are not sufficiently different to make it possible to allocate distinct peaks to these defects. Inasmuch as lowering the annealing pressure results in increasing concentration of point defects, peak B, which represents the perfect TiO_2 structure, shrinks when the films are annealed under lower ambient pressures.

The results of photocatalytic experiments under ultraviolet light are shown in figure 9. As is seen in the inset of this figure, the concentration of 4CP decreases with illumination time showing that the 4CP is being decomposed. It should be noted that the curve 'No catalyst' corresponds to the experiment where no sample was used as a catalyst and only the 4CP solution was irradiated by the UV light. Since no appreciable concentration change is seen in this experiment,

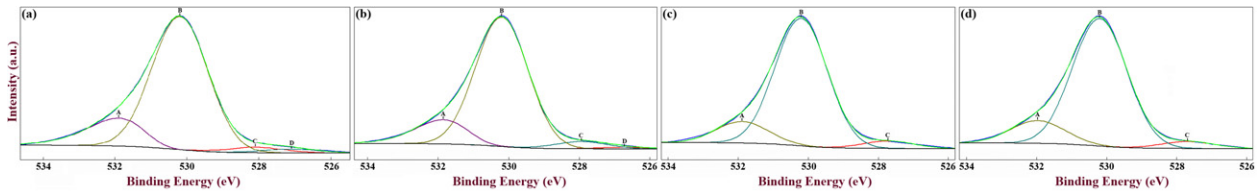

Figure 8. XPS O(1s) core level binding energies in the TiO_2 films annealed under pressures of (a) 5×10^{-6}, (b) 5×10^{-3} and (c) 5×10^1 Torr, and (d) in the un-annealed sample.

Table 1. Portion of the XPS peaks for different oxygen pressures.

XPS peak		Pressure			
		Un-annealed	5×10^{1} Torr	5×10^{-3} Torr	5×10^{-6} Torr
		Portion (%)			
O(1s)	A	14.6	13.8	15.3	17.0
	B	79.9	81.4	79.3	77.4
	C	4.5	4.8	4.4	3.3
	D	—	—	1.0	2.3

Table 2. Photocatalytic reaction rate constants (min^{-1}) as a function of the annealing pressure.

Illumination	Annealing pressure				
	No catalyst	5×10^{-2} Torr	5×10^{-3} Torr	5×10^{-4} Torr	5×10^{-6} Torr
Ultraviolet	0.000 11	0.006 67	0.007 74	0.010 70	0.009 73
Visible		0.001 51	0.005 07	0.007 28	0.006 16

it can be deduced that in the other experiments, which were performed using a catalyst, the 4CP was degraded by the photoactivated rutile films. To quantitatively compare the photocatalytic activity of the layers, the photocatalytic reaction rate constants (k) should be calculated. Since the photocatalytic decomposition of the 4CP solution agrees with pseudo-first-order kinetics, the constant (k) can be calculated by the equation $\ln(C/C_o) = -kt$ (where C_o is the initial concentration of 4CP at $t = 0$ and C represents the concentration of 4CP at later times t). The quantity $\ln(C_o/C)$ versus irradiation time is plotted for all samples. Straight lines, whose slopes represent k, indicate that the degradation of 4CP is a first-order reaction. The reaction rate constants (listed in table 2) show that the photocatalytic activity increases when the catalysts are annealed under lower pressures, namely 5×10^{-4} Torr. It has already been shown that the defect content increases at lower annealing pressures. The structural defects, namely V_O, trap photogenerated electrons and, consequently, enhance the charge separation so that positive holes, which are prerequisite for photocatalytic decomposition of 4CP, can participate in reactions without any recombination. Furthermore, oxygen vacancies at the TiO_2 surface promote the adsorption of molecules. However, the sample annealed under a pressure of 5×10^{-6} Torr displays an apparently abnormal behavior, as its photocatalytic efficiency is lower than that for the sample annealed under 5×10^{-4} Torr. The reason may be formation of deep level point defects. The energy levels of defects are influenced by their concentration; that is, the environment around the defects can affect the energy band edges of defects. As was already shown, the concentration of defects is increased by low-pressure annealing leading to the formation of deep level defects acting as recombination centers. The efficiency of a photocatalytic process is determined by two factors: the absorption capacity of the semiconductor, which dictates the initial number of carriers, and the time required for the carrier to reach the surface and participate in the photocatalytic reactions (equations (1)–(6)). Electron–hole recombination is an important competing process, since it decreases the carrier mobility and prevents them from reaching to the

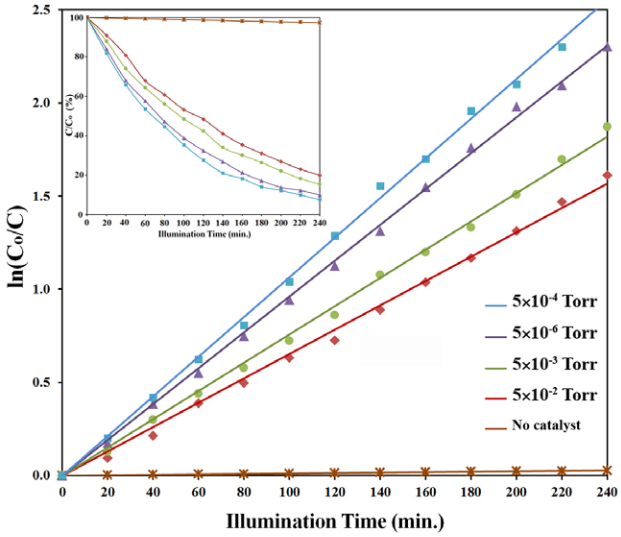

Figure 9. The photocatalytic activity of the rutile TiO_2 films under ultraviolet illumination.

surface. We think that the charge recombination at the deep level defects is responsible for diminishing the photocatalytic efficiency. Meanwhile, the film annealed under a pressure of 5×10^{-6} Torr had a smoother surface (figure 5) and, hence, a smaller surface area where photocatalytic reactions occur, resulting in a lower photocatalytic efficiency.

According to the literature [25] and our results, the following reactions are put forward for photocatalytic degradation of 4CP over defected rutile TiO_2 catalyst:

$$TiO_2 + h\upsilon \longrightarrow e^- + h^+ \quad (13)$$

$$e^- + V_O \longrightarrow \text{trapped electrons} \quad (14)$$

$$h^+ + H_2O \longrightarrow H^+ + {}^{\bullet}OH \quad (15)$$

$$2C_6H_5OCl + 13O_2 \xrightarrow{{}^{\bullet}OH} 12CO_2 + 4H_2O + 2HCl. \quad (16)$$

Reaction (16) is schematically illustrated in figure 10.

The photocatalytic performance of the rutile films under visible light was also investigated, the results of which are

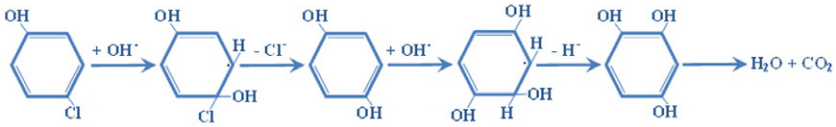

Figure 10. Schematic illustration of photo-degradation of 4-chlorophenol on TiO_2 films.

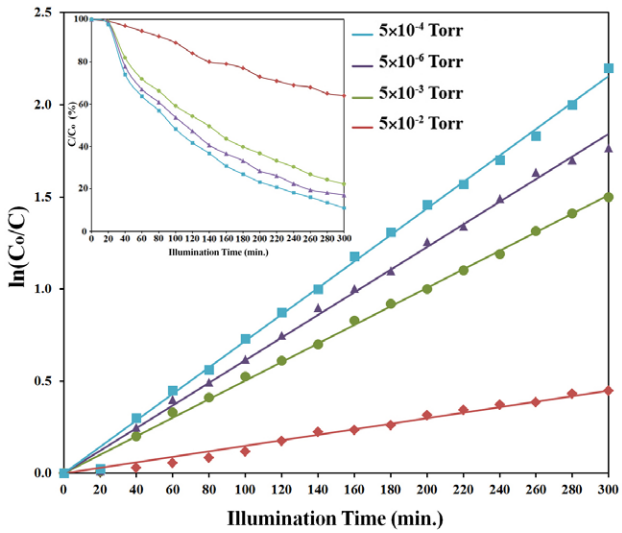

Figure 11. The photocatalytic activity of the rutile TiO_2 films under visible illumination.

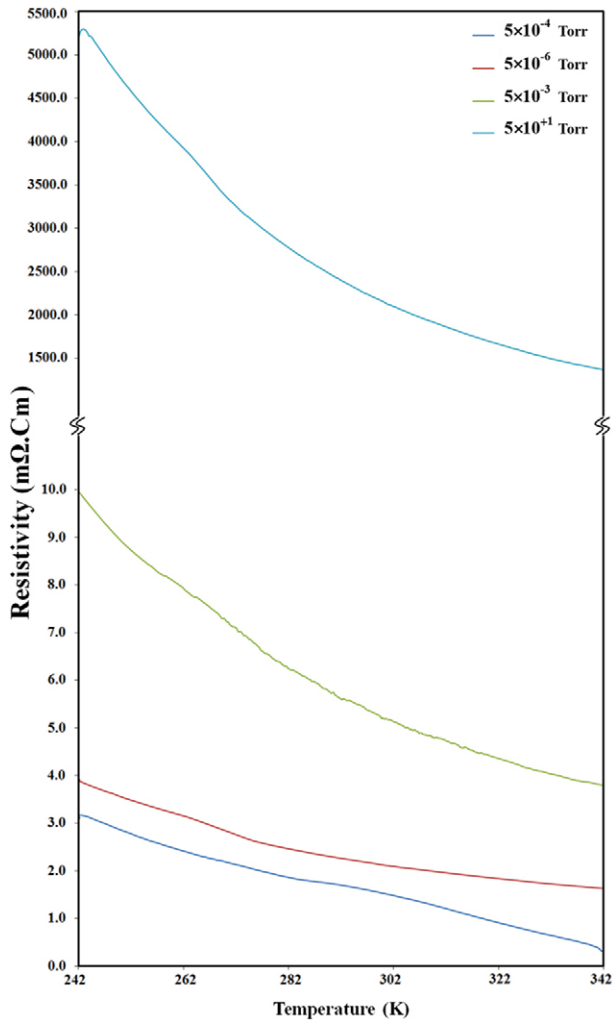

Figure 12. The dependence of the electrical resistivity on the annealing pressure.

shown in figure 11. The corresponding photocatalytic reaction rate constants are listed in table 2. As is observed, the layers are photoactive even under low energy visible irradiation. As was discussed earlier, the films annealed under low oxygen pressures have a narrow band gap and, therefore, they are photo-responsive under visible light. The reason behind this behavior is that the Ti_i atom spontaneously donates three electrons to the surrounding lattice Ti ions and forms a Ti^{3+} ion with a single electron localized on a 3d shell. In addition, the formation of each V_O defect results in the formation of two Ti^{3+} in the lattice, as explained earlier. The presence of both lattice and interstitial Ti^{3+} ions leads to the creation of new energy states (about 1–1.5 eV below the conduction band) within the band gap of TiO_2 [13, 18]. The electrons are initially excited from the valence band to the defect energy levels and, then, to the conductance band of titania.

We proposed that the lower photocatalytic efficiency of the film annealed at 5×10^{-6} Torr originated from its lower carrier mobility. To further confirm this conjecture, the electrical properties of the layers were investigated. The variation of the electrical resistivity of the annealed rutile TiO_2 films with temperature for different oxygen pressures is displayed in figure 12 where a strong dependence of resistivity on oxygen pressure is apparently observed. It is seen that the resistivity increases by about three orders of magnitude as the oxygen pressure increases from 5×10^{-6} to 5×10^{1} Torr. As discussed earlier, increased oxygen diffusion at high oxygen pressures decreases the concentration of oxygen vacancies and titanium interstitials and, thus, suppresses the carrier concentration and conductivity. It is also seen that the electrical resistivity increases when the annealing pressure decreases from 5×10^{-4} to 5×10^{-6} Torr. Indeed, the film annealed under a pressure of 5×10^{-6} Torr exhibited lower photocatalytic efficiency and electrical conductivity as compared to the film annealed under 5×10^{-4} Torr. The reason behind this behavior is that the carrier mobility is determined by different scattering mechanisms, including scattering by grain boundaries and intrinsic defects. As was already deduced, the concentration of defects increases significantly at very low pressures, e.g. 5×10^{-6} Torr, leading to appreciable scattering and trapping phenomena that, in turn, increase the resistivity.

4. Conclusion

Visible-light-responsive rutile TiO_2 films were developed by a PLD process followed by vacuum annealing, where it is envisaged that the point defects play a crucial role by introducing mid-band energy levels. The layers were single crystalline and the epitaxial relationship between the film and the substrate was shown to be $(100)_R \parallel (0001)_S$, rutile $[001]_R \parallel [10\bar{1}0]_S$ and $[010]_R \parallel [1\bar{2}10]_S$. Epitaxial growth and the formation of an atomically sharp interface between the rutile film and the substrate were confirmed by STEM as well. The maximum photocatalytic reaction rate constants for degradation of 4-chlorophenol were determined as 0.0107 and 0.0072 min^{-1} under UV and visible illumination, respectively. It was also shown that the electrical resistivity increased by three orders of magnitude when the annealing pressure was increased from 5×10^{-4} to 5×10^{1} Torr. Thus, the photocatalytic activity of titania films can be tuned by controlling the annealing pressure, hence enabling a variety of environmental remediation processes.

Acknowledgment

This research was supported by the National Science Foundation (NSF).

References

[1] Du Y, Fu Q S, Li Y and Su Y 2011 *J. Hazard. Mater.* **186** 491
[2] Cheng Y, Sun H, Jin W and Xu N 2007 *Chem. Eng. J.* **128** 127
[3] Theurich J, Lindner M and Bahnemann D W 1996 *Langmuir* **12** 6368
[4] Fujishima A and Honda K 1972 *Nature* **238** 37
[5] Pian X T, Lin B Z, Chen Y L, Kuang J D, Zhang K Z and Fu L M 2011 *J. Phys. Chem.* C **115** 6531
[6] Kurtoglu M T, Longenbach T, Sohlberg K and Gogotsi Y 2011 *J. Phys. Chem.* C **115** 17392
[7] Dong F, Guo S, Wang H, Li K and Wu Z 2011 *J. Phys. Chem.* C **115** 13285
[8] Bayati M R, Moshfegh A Z and Golestani-Fard F 2010 *Appl. Catal.* A **389** 60
[9] Bayati M R, Moshfegh A Z and Golestani-Fard F 2010 *Mater. Lett.* **64** 2215
[10] Bayati M R, Golestani-Fard F and Moshfegh A Z 2011 *Mater. Chem. Phys.* **128** 427
[11] Bayati M R, Moshfegh A Z and Golestani-Fard F 2010 *Electrochim. Acta* **55** 3093
[12] Peng H 2008 *Phys. Lett.* A **372** 1527
[13] Finazzi E, Valentin C D and Pacchioni G 2009 *J. Phys. Chem.* C **113** 3382
[14] Zhuang J, Dai W, Tian Q, Li Z, Xie L, Wang J and Liu P 2010 *Langmuir* **26** 9686
[15] Campbell S A, Gilmer D C, Wang X C, Hsieh M T, Kim H S, Gladfelter W L and Yan J 1997 *IEEE Trans. Electron. Devices* **44** 104
[16] Kroger F A and Vink H J 1956 *Solid State Physics* (New York: Academic) p 307
[17] Nowotny M K, Bak T and Nowotny J 2006 *J. Phys. Chem.* B **110** 16270
[18] Nowotny M K, Sheppard L R, Bak T and Nowotny J 2008 *J. Phys. Chem.* C **112** 5275
[19] Bak T, Nowotny J, Rekas M and Sorrell C C 2003 *J. Phys. Chem. Solids* **64** 1057
[20] Chan S W 1994 *J. Phys. Chem. Solids* **55** 1137
[21] Bayati M R, Joshi Sh, Molaei R, Narayan R J and Narayan J 2012 *J. Solid State Chem.* **187** 231
[22] Bayati M R, Molaei R, Narayan R J, Narayan J, Zhou H and Pennycook S J 2012 *Appl. Phys. Lett.* **100** 251606
[23] Jung H S, Lee J K, Lee J, Kang B S, Jia Q, Nastasi M, Noh J H, Cho C M and Yoon S H 2008 *Langmuir* **24** 2695
[24] Martyanov I N, Berger T, Diwald O, Rodrigues S and Klabunde K J 2010 *J. Photochem. Photobiol.* A **212** 135
[25] Cheng Y, Sun H, Jin W and Xu N 2007 *Chem. Eng. J.* **128** 127